J Electroceram (2009) 22:346–351
DOI 10.1007/s10832-008-9513-3

Multilayer piezoelectric linear ultrasonic motor for camera module

Dong-Soo Paik · Kyoung-Ho Yoo · Chong-Yun Kang · Bong-Hee Cho · Sahn Nam · Seok-Jin Yoon

Received: 31 August 2007 / Accepted: 16 April 2008 / Published online: 18 June 2008

Abstract Piezoelectric linear ultrasonic motors have been widely studied for auto focusing devices of digital cameras and cellular phones due to their simple structure. A piezoelectric motor operated at low voltages, not achievable using bulk piezoelectrics, is required for the camera module of cellular phone. In this study, a tiny piezoelectric linear motor was fabricated and its dynamic properties at low voltages were analyzed. To reduce the driving voltage, thin multilayer ceramics fabricated by a tape casting method were applied to the motor. The proper number of layers of the piezoelectric element was determined by ATILA simulation program. As a result of the simulation, the largest displacement of the shaft was observed at 21 layers. Characteristics of the motor were analyzed with respect to applied voltages and frictional forces between the mobile element and shaft. Velocity and force of the motor increased with increasing applied voltage. The motor exhibited a velocity of 10.9 mm/s and a thrust force of 110 mN at a frictional force of 62.5 mN and an applied voltage of 10 $V_{p\text{-}p}$.

Keywords Piezoelectric ceramics · Frictional force · Multilayer actuator · Linear motor

D.-S. Paik · K.-H. Yoo · C.-Y. Kang · S.-J. Yoon (✉)
Thin Film Materials Research Center, KIST,
Seoul, South Korea
e-mail: sjyoon@kist.re.kr

B.-H. Cho
Department of Electrical Engineering, The University of Suwon,
Hwasung, South Korea

D.-S. Paik · S. Nam
Department of Materials Science Engineering, Korea University,
Seoul, South Korea

1 Introduction

Ultrasonic motors are attractive for the application to camera modules of imaging devices such as personal/mobile computers, mobile telephones and PDAs. In particular, various types of ultrasonic motors with compact size have been suggested to have a wide range of optical device applications. The compact ultrasonic motor exhibits higher flexibility compared to that of the conventional electromagnetic motors whose efficiency significantly decreases with miniaturization [1–3]. It is entirely different from conventional motors such as electromagnetic motors that utilize the interactions between the electromagnetic fields. Furthermore, it has the following advantages compared with the conventional motors; (1) stable operation with proper velocity and torque, which is suited for direct drive without any gears for reduction of speed or converting mechanisms for changing operating directions, (2) quick response and excellent controllability of starting, stopping and reversing, (3) small size and light weight, and (4) absence of any electronic disturbances.

A new tiny ultrasonic motor using flexural vibration of a piezoelectric bimorph was previously reported elsewhere [4]. However, the operating voltage of the motor approaching to 60 $V_{p\text{-}p}$ was too high to apply for a camera module of a mobile phone. It is therefore necessary for a piezoelectric actuator to be operated using a simple circuit including dc to ac conversion without any amplifying function. In general, the output voltage of ~4 V_{dc} supplied by a mobile phone battery can be easily modified to 10 $V_{p\text{-}p}$ without amplification.

In this article, to realize a low-voltage driven motor for application in the camera module, a multilayer actuator suited to the tiny motor was employed [4]. After simulating the structure and dimension of the motor by ATILA,

dynamic properties of the manufactured motor such as velocity, thrust force, and displacement have been investigated with respect to the number of ceramic layers, applied voltage, and frictional force.

2 Construction and principle

2.1 Construction of piezoelectric linear motor

The tiny piezoelectric linear motor using an inertia movement consisted of three parts; a transducer, a shaft, and a mobile element. The transducer consisted of a bimorph comprising two multilayer piezoelectric ceramics and a metal disk glued together by epoxy as shown in Fig. 1. The multilayer piezoelectric ceramic was fabricated by a tape casting method and sintered at 900 °C for 1 h. The thicknesses of each ceramic layer and internal electrode were ~45 and ~8 μm, respectively. The transducer is driven by a saw-tooth electrical voltage applied to the electrode on the piezoelectric disk. Table 1 shows dimension of the transducer. The multilayer piezoelectric ceramic disk generates one of the transverse length extension modes presenting a periodical extension and contraction along the radius direction of the piezoelectric ceramic disk. The transducer also comprises a rectangular elastic plate to enhance the reliability because the piezoelectric bimorph without the elastic plate can be broken under a consecutive vibration. The cap used to decrease parasitic vibrations and to increase displacement of the transducer in the previous articles [4–6] was removed in the presented motor (Fig. 2).

2.2 Operating principle of piezoelectric linear motor

A linear motion of the manufactured motor is generated by means of an inertia force induced by applying a saw-tooth electrical voltage as shown in Fig. 3. In association with the inertia force, the motor can be linearly operated by a frictional force between the shaft and the mobile element. A preload was applied between the shaft and mobile element using a spring to acquire a proper frictional force. The movement of the mobile element loaded to the shaft is

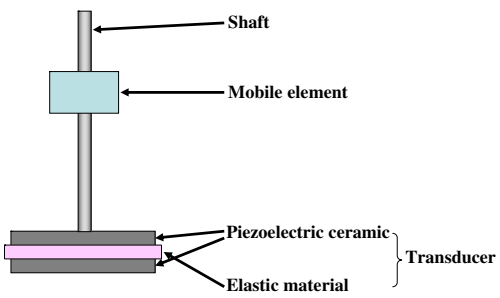

Fig. 1 Structure of the multilayer piezoelectric linear motor

Table 1 Dimension of the transducer of the manufactured motor.

Transducer part	Piezoelectric ceramic Hard type	Elastic material Brass
Size (mm^2)	3×7	4×11
Thickness (μm)	45	100
Poling direction	*z*-Axis	

depicted in Fig. 3. The left end of shaft and the piezoelectric element are initially located at the position of $x=0$ as shown in Fig. 3 (a). The distance between the left end of shaft and the mobile element is represented as Sa. At this moment, the electrical potential is not applied as shown in Fig. 3 'a'. When the electrical potential is applied from zero to the maximum electrical potential as same as a–b interval of Fig. 3, the shaft and the mobile element move together smoothly and linearly from (a) to (b) along a distance 'A'. As the electrical potential of b–c interval, abruptly falling down to −Va, is applied to the piezoelectric element, the piezoelectric element exhibits the maximum rate of displacement of '2A' towards the opposite direction and then the shaft only moves along a distance '2A' as shown in Fig. 3 (b) and (c). It can be summarized that the shaft and the mobile element are simultaneously moved in the forward direction by the frictional force and then the shaft only is slipped by the inertia force under the saw-tooth type electrical potential, still maintaining the moved position of the mobile element ($x = S_b$). When the applied electrical potential is linearly raised from −Va to Va once again as shown in c–d interval of Fig. 3, the shaft moves with the mobile element along a distance '2A' as shown in Fig. 3 (c) and (d). When the electrical potential of d–e interval is applied, the moving element and the shaft exhibit a movement the same as the one generated in b–c interval

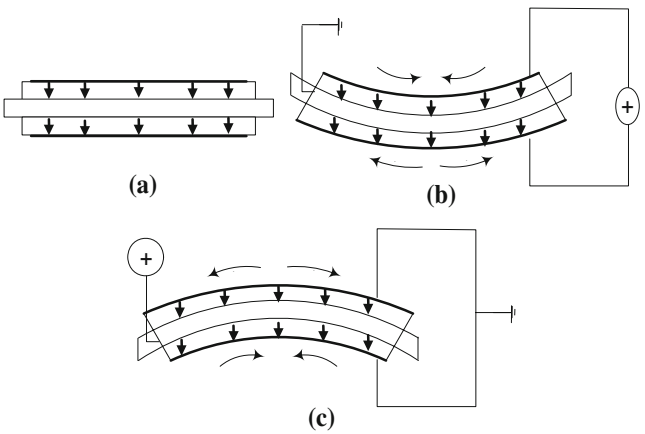

Fig. 2 Polarization direction and vibration configuration of transducer for multilayer piezoelectric linear motor; (**a**) original vibration configuration and polarization direction (*downward arrow*) of the transducer, and (**b**), (**c**) downward and upward flexural vibration of the transducer according to the electric field, respectively

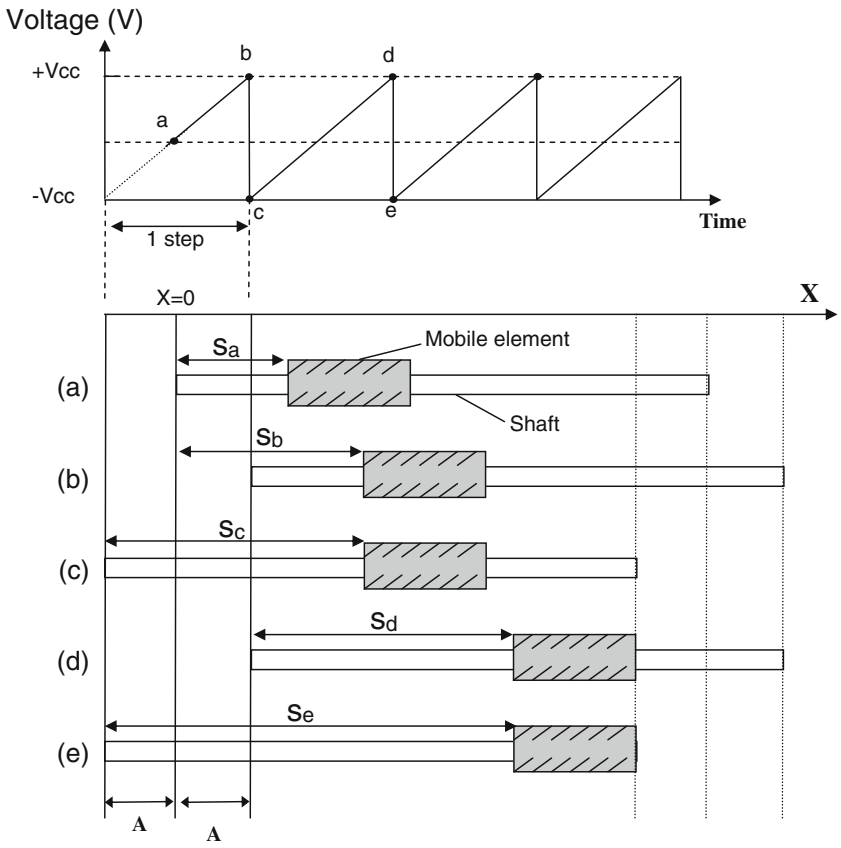

Fig. 3 Operating principle of the linear motion for the piezoelectric motor

as described above. As a result, the piezoelectric element and the shaft always move together regardless of the voltage ramping ratio, and the mobile element can linearly move only while the voltage is rapidly ramped up. It can be also possible to shift the mobile element in the opposite direction by changing the slope of electrical potential to fast ascending and slow descending. It is evident from Fig. 3 that the mobile element continuously moves from left to right ends as it repeats this kind of motion [4–5].

3 Finite element method analysis

The finite element method ATILA is used for designing piezoelectric devices, which takes into account the coupling between the transducer mechanical structure and the surrounding medium [7–11]. Finite element analysis of the actuator is very important for designing a novel ultrasonic linear motor, because it provides some information such as possible driving frequency and performance of the motor. We can evaluate the characteristics of the piezoelectric motor based on ATILA. The dimension of the transducer of the motor is summarized in Table 1 and various properties of the piezoelectric material for the simulation are listed in Table 2. The boundary condition of the transducer was established as a free state to generate a flexural vibration in the transducer of the motor. The flexural vibration of the piezoelectric element finally creates the linear movement of the proposed motor. Fig. 4 shows the modeled normalized displacement of the shaft vs. number of layers of the multilayer ceramic with respect to the maximum displacement observed at the specimen consisted of piezoelectric ceramic sheets of 21 layers for each piezoelectric element. With increasing number of layers, relatively large displacement of the shaft was observed. However, the displacement slightly decreased as the number of layers increases over 21. It may be assumed that the piezoelectric bimorph having the piezoelectric layers of over 21 presented not a pure flexural vibration but a mixed vibration combined with a thickness mode. The displacement therefore decreased with increasing number of layers more than 23. As a result of the simulation result, 21

Table 2 Properties of the piezoelectric material.

Properties	Value
Relative dielectric constant, $\varepsilon_{33}/\varepsilon_0$	1,300
Piezoelectric charge constant, d_{33} ($\times 10^{-12}$ m/V)	593
Piezoelectric voltage constant, g_{33} ($\times 10^{-3}$ m/V)	28
Mechanical quality factor, Q_m	1,600
Density, ρ ($\times 10^3$ kg/m^3)	7.5

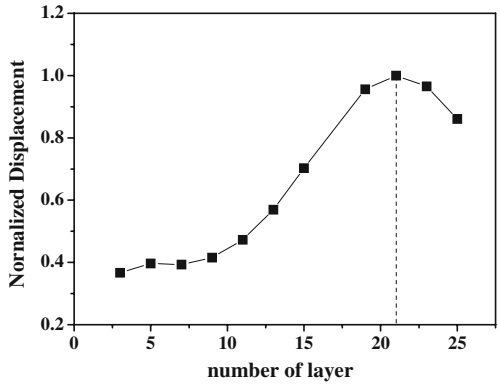

Fig. 4 Displacement of the shaft according to number of layers of multilayer actuator by ATILA simulation

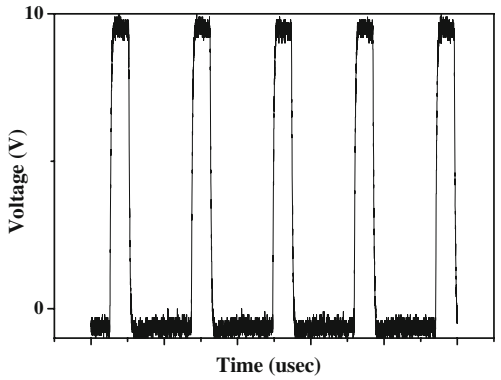

Fig. 6 Voltage waveform applied to the multilayered tiny piezoelectric linear motor

layers for each piezoelectric element were determined to be the proper number of layers for the proposed piezoelectric linear motor. Therefore, the bimorph piezoelectric transducer as shown in Fig. 1 comprises total 42 piezoelectric layers and its thickness approaches to 2,500 μm including the internal electrodes and the elastic plate.

4 Experimental

The experimental setup for measurement of the piezoelectric motor is illustrated in Fig. 5. A signal generator (WF1943A by NF) and a high frequency amplifier (NF4010) were used as the drive power supply. Electrical behavior of the motor was measured with a power meter (WT1600 by Yokogawa). Dynamic characteristics of the motor were investigated under rectangular voltage waveforms with a duty ratio of 23 to 77 as shown in Fig. 6. It is expected that the rectangular waveform makes the piezoelectric element work to be identical with the saw-tooth waveform as shown in Fig. 3 since the piezoelectric materials show slower charging time compared to the rising time of electrical signal. Variation of electric properties with respect to load resistance and driving frequency were monitored with an oscilloscope (TDS3032 by Tektronix).

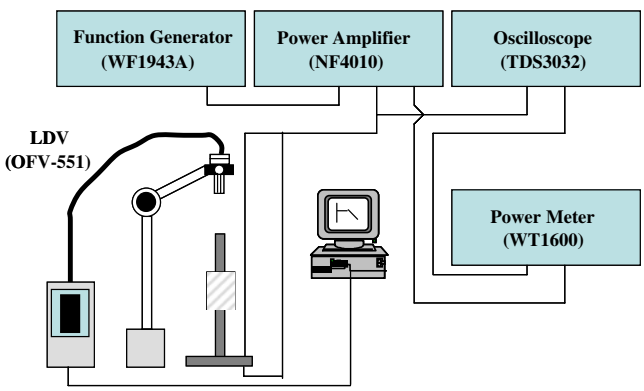

Fig. 5 Measurement set-up for the piezoelectric linear motor

Transient response and displacement of the motor were measured using a laser doppler vibrometer (VDD-Z-011 and OFV-551, by Polytec PI). Actuating force of the mobile element was measured by a digital force gauge (DPS-5 by IMADA).

5 Results and discussion

Figure 7 shows resultant displacement characteristics of the shaft under the rectangular input voltage. When the rectangular voltage is applied, the induced displacement with a time delay was observed. The displacement with slow increase and fast decrease, identical with the behavior under the saw-tooth waveform, was observed. Therefore, the rectangular waveform generated by a simple PWM is also effective to obtain an inertia force for the piezoelectric linear motor. It is also supposed to be caused by the capacitive charging and delay time of the piezoelectric ceramic. It is obviously seen that the motor has the inertia behavior, showing that the shaft shifts slowly in one direction and rapidly in the opposite direction.

Figure 8 shows displacement of the shaft and velocity of the mobile element when the rectangular voltage waveform is applied to the transducer. Both the displacement and

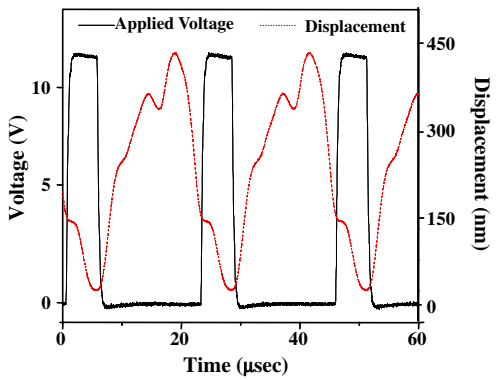

Fig. 7 Displacement characteristics of the shaft for rectangular input voltage

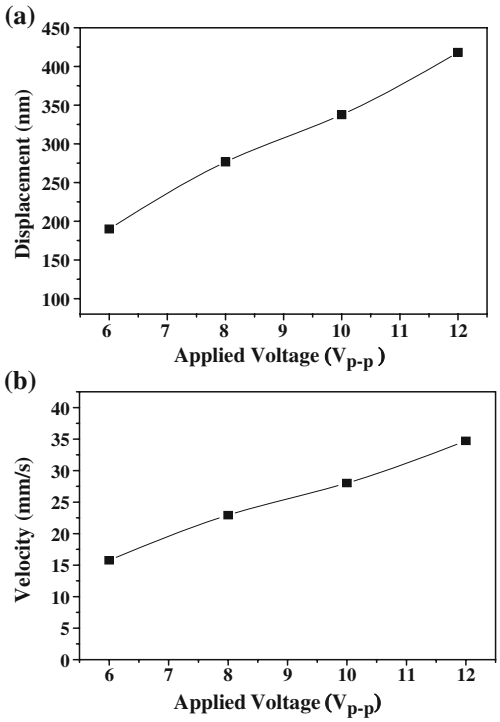

Fig. 8 Dynamic properties of the motor as a function of applied voltage; (**a**) displacement of the shaft and (**b**) velocity of the mobile element

velocity increased with increasing the applied voltage. When the voltage of 10 V_{p-p} applicable to auto focusing devices was applied, the displacement of shaft and the velocity of mobile element were 337.7 nm and 28.0 mm/s, respectively. It is noted that these values satisfy the specification for commercialization.

The highest velocity and thrust force according to the number of ceramic layers were measured as shown in Fig. 9. The maximized velocity and thrust force was measured at 21 layers. It is in good agreement with the simulation result as shown in Fig. 4.

The velocity and the thrust force were also measured as a function of frictional force between the shaft and the mobile element at an applied voltage of 10 V_{p-p} as shown in

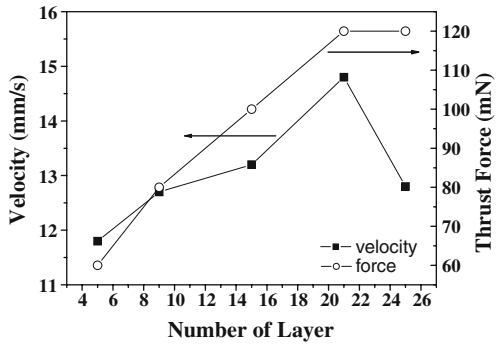

Fig. 9 Velocity and thrust force of the motor according to the number of ceramic layers at an applied voltage of 12 V_{p-p} and a frictional force of 62.5 mN

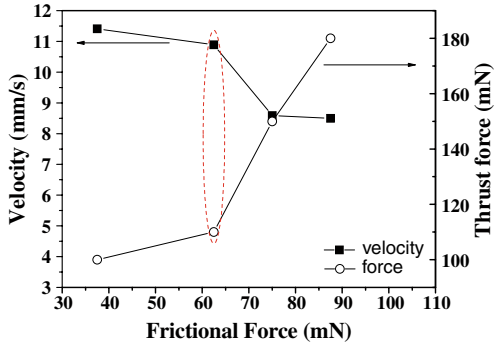

Fig. 10 Velocity and thrust force of the motor according to frictional force between shaft and mobile element at an applied voltage of 10 V_{p-p}

Fig. 10. The dynamic behavior of the manufactured motor was obviously affected by the frictional force, i.e., both the velocity and the thrust force varied under different frictional force. The increased frictional force resulted in the decreased velocity and the increased thrust force.

The manufactured motor exhibited the fastest velocity of 14.8 mm/s and the largest thrust force of 120 mN at a frictional force of 62.5 mN and an applied voltage of 12 V_{p-p} as shown in Fig. 11. Both the velocity and the thrust force tend to linearly increase with increasing the applied voltage. Desirable conditions for the satisfactory velocity and thrust force to apply the camera module were determined to be 10.9 mm/s and 110 mN at a frictional force of 62.5 mN and an applied voltage of 10 V_{p-p}.

6 Conclusions

This paper presents dynamic properties of the piezoelectric linear motor using the flexural vibration for lower driving voltage and simple structure. The optimum number of piezoelectric ceramic layers providing the best displacement quality was determined to be 21 layers by ATILA simulation and consequently the simulated results were applied to the practical motor fabrication. The velocity and the thrust force of the mobile element representing important parameters for

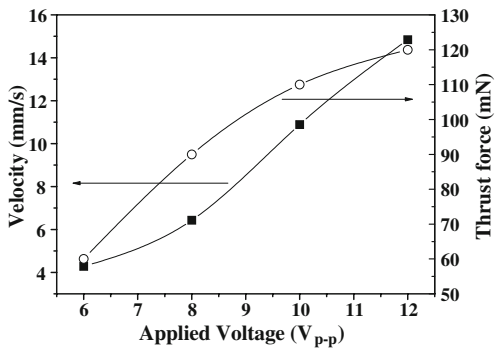

Fig. 11 Velocity and thrust force of the motor according to the applied voltage at a frictional force of 62.5 mN

motors, increased with the increasing applied voltage. For practical use, the optimum velocity and force of the mobile element were 10.9 mm/s and 110 mN, respectively, at a voltage of 10 $V_{p\text{-}p}$ and a frictional force of 62.5 mN. These results confirm the suitability of the multilayer piezoelectric linear motor for application to the cellular phone camera module.

References

1. K. Uchino, B. Koc, Compact piezoelectric ultrasonic motors, JPL/NASA Biomorphic Explorers Conference (1998)
2. S. Dong, S.P. Lim, K.H. Lee, J. Zhang, L.C. Lim, K. Uchino, Piezoelectric ultrasonic micromotor with 1.5 mm diameter. IEEE Trans. Ultrason. Ferroelectr. Freq. Control. **50**(4), 361 (2003). DOI 10.1109/TUFFC.2003.1197958
3. S. Cagatay, B. Koc, K. Uchino, A 1.6-mm, metal tube ultrasonic motor. IEEE Trans. Ultrason. Ferroelectr. Freq. Control. **50**(7), 782 (2003). DOI 10.1109/TUFFC.2003.1214498
4. H.-P. Ko, S. Kim, J.-S. Kim, S.-J. Yoon, Wear and dynamic properties of piezoelectric ultrasonic motor with frictional materials coated stator. Mater. Chem. Phys. **90**, 391 (2005). DOI 10.1016/j.matchemphys.2004.09.037
5. H.-P. Ko, S. Kim, C.-Y. Kang, S.-J. Yoon, Optimization of a piezoelectric linear motor in terms of the contact parameters. Mater. Chem. Phys. **90**, 322 (2005). DOI 10.1016/j.matchemphys.2004.09.041
6. H.-P. Ko, S. Kim, S.N. Borodinas, S.-J. Yoon, A novel tiny ultrasonic linear motor using the radial mode of a bimorph. Sens. Actuators. **125**, 477 (2005). DOI 10.1016/j.sna.2005.07.014
7. J. Zhang, A.-C. Hladky-Hennion, W.J. Hughes, R.E. Newnham, Modeling and underwater characterization of cymbal transducers and arrays. IEEE UFFC. **48**(2), 560–568 (2001)
8. MAGSOFT Corporation, ATILA Version 5.1X User's Manual, Troy, NY: MAGSOFT Corp.,1997.
9. A.-C. Hladky-Hennion, Finite element analysis of the propagation of acoustic waves in waveguides. J. Sound Vib. **192**(2), 19–136 (1996). DOI 10.1006/jsvi.1996.0349
10. A.-C. Hladky-Hennion, P. Langlet, M. de Billy, Finite element analysis of the propagation of acoustic waves along waveguides immersed in water. J. Sound Vib. **200**(4), 519–530 (1997). DOI 10.1006/jsvi.1996.0749
11. A.-C. Hladky-Hennion, P. Langlet, R. Bossut, M. de Billy, Finite element modeling of radiating waves in immersed wedges. J. Sound Vib. **212**(2), 265–274 (1998). DOI 10.1006/jsvi.1997.1408